



Removal of Congo Red Anionic Dye from Aqueous Solution Using Polyaniline/TiO₂ and Polypyrrole/TiO₂ Nanocomposites: Isotherm, Kinetic, and Thermodynamic Studies

M. Tanzifi*, K. Karimipour, M. Najafifard, S. Mirchenari

Department of Chemical Engineering, Faculty of Engineering, University of Ilam, Ilam, Iran

PAPER INFO

Paper history:

Received 17 August 2016

Received in revised form 23 September 2016

Accepted 11 November 2016

Keywords:

Polyaniline
Polypyrrole
Titanium Dioxide
Adsorption
Kinetic Studies
Isotherm
Thermodynamic
Congo Red

ABSTRACT

The present study seeks to investigate the capacity of polyaniline/titanium dioxide (PAn/TiO₂) and Polypyrrole/titanium dioxide (PPy/TiO₂) nano-adsorbents to adsorb Congo red anionic dye (CR) from aqueous solution. The variables effective in CR adsorption, including adsorbent dose, pH of the solution, contact time, initial dye concentration, and temperature were examined. The study yielded the result that a decrease in pH increases the adsorption capacity of both nano-adsorbents. The adsorbent dose and optimum contact time of PAn/TiO₂ and PPy/TiO₂ nano-adsorbents were [0.1 gr and 20 min] and [0.2 gr and 60 min], respectively. The adsorption kinetics data was estimated with the pseudo-first-order, pseudo-second-order, and Weber–Morris equations. Kinetic studies showed that the CR adsorption process onto both nano-adsorbents followed the pseudo-second-order kinetics model, which indicates that the adsorption process is chemisorption-controlled. Langmuir, Freundlich, Temkin, and Dubinin–Radushkevich Isotherms were applied to the adsorption data to estimate the maximum adsorption capacity as well as the intensity and energy of adsorption. The experimental data were best represented by Freundlich isotherm model compared to the other models. Analysis of data with Dubinin–Radushkevich isotherm showed that the adsorption of CR onto both nano-adsorbents is a chemisorption process. Moreover, Thermodynamic parameters such as ΔG , ΔH , and ΔS were calculated. The results showed that the adsorption of CR onto both nano-adsorbents was spontaneous and exothermic.

doi: 10.5829/idosi.ije.2016.29.12c.04

1. INTRODUCTION

Dye is one of the pollutants posing dangerous threat to the environment and human health as well. They are widely used in different industries such as textile industry. Dye removal from industrial wastewater is a difficult process. In other words, dye is difficult to treat, consequently, these pollutants along with the other industrial wastewater find their way to the environment. 15 to 20% of the dye used in textile factories enters the wastewater stream [1]. Dyes are organic compounds containing one or more benzene rings. Due to their toxicity and late hydrolysis, such materials cause irreparable damage to the environment and humans, namely cancer, mutagenesis, etc [2]. Therefore,

wastewater containing dyestuff is considered as one of the serious threats to humans' health and the environment [3, 4]. Due to their capacity to remove highly persistent pollutants efficiently, adsorption techniques have recently been taken into consideration. In so doing, pollutant removal was done through binding it to a solid organic material or inorganic matrix; the binding can be done by ion exchange, electrostatic, vander Waals, complexation, etc.. The process of dye removal from wastewater is dependent on different conditions such as adsorbent particle size, contact time, temperature, environment pH, and the presence of surfactants and metals [5]. The adsorption process is considered to be an effective method only if an efficient adsorbent with high adsorption capacity is used. Nano-sized materials, due to their high specific surface area, high reactivity, and high adsorption and

*Corresponding Author's Email: m.tanzifi@ilam.ac.ir (M.Tanzifi)

desorption capacity, have many applications in environmental remediation and adsorption of contaminants from wastewater [6-11]. Different adsorbents, including Mn-doped Fe₃O₄ nanoparticle-loaded activated carbon (Mn-Fe₃O₄-NP-AC) [12], activated carbon/ γ -Fe₂O₃ nanocomposite [13], Fe₃O₄/MgO nanoparticles [14], iron nanoparticles [15], Cu_{0.5}Mn_{0.5}Fe₂O₄ nanospinels [16], have been examined for the purpose of dye removal from wastewater. Since conductive polymers were identified, a great bulk of studies has been carried out in the realm of their applications. Such compounds can be used in rechargeable batteries and capacitors, sensors, and fiber coating as well [17-19]. Conductive polymers have recently been considered as adsorbents regarding the analysis of environmental pollutants [20]. Some of the conductive polymers such as polyaniline and polypyrrole are synthesized facilely and enjoy high environmental and thermal stability, conductivity, and bio-compatibility; that is why these compounds have come into the focus of many researchers [21-24]. Polyaniline and polypyrrole have ion exchange properties and are capable of removing various pollutants including heavy metals and dyes from aqueous solutions. Ion exchange properties of these polymers are dependent on different conditions, including polymerization conditions, the presence of stabilizer, the size and type of the dopant, and polymer size. Furthermore, conductive polymers feature considerable positive sites that can remove pollutants such as anionic dyes through Coulomb forces [25]. Combining polyaniline and polypyrrole with some materials including metallic nanoparticles increases its adsorption capacity. The results of the study conducted by Shانهsaz et al. showed that iron oxide nanoparticles covered by polypyrrole are highly efficient in adsorbing reactive blue 19 (RB19) dye. The maximum adsorption capacity was reported to be 112.36 mg/g [26]. In the study carried out by Salem et al., polyaniline-silver nanocomposite was used as an adsorbent for the removal of brilliant green dye from aqueous solution. It was also found that adsorption data fits the Langmuir isotherm [27]. Khalili et al. came to the result that polyaniline/Sb₂O₃ nanocomposite are capable of removing pb(II) from aqueous media [28].

Titanium dioxide nanoparticles are regarded as one of the most widely used metal particles. TiO₂ NPs can be used in membranes, gas sensors, solar cells, battery and catalyst, as well as dye degradation [29-34]. These particles, used as nano-fillers, lead to the modification of the polymeric network, which consequently, increases the surface area of the adsorbent allowing adsorbates to be adsorbed. Fabrication of conductive polymer composites (CPCs) through TiO₂ has been reported [35, 36]. Congo red is one of the diazo dyes. It is soluble in water and exists in wastewater of some industries such as textile, leather, printing and paint.

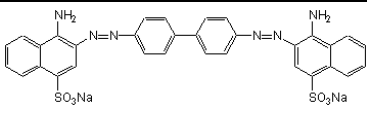
This dye is toxic, carcinogenic and mutagenic and causes some serious problems such as respiratory and gastrointestinal diseases and irritation of skin and eye. So removing this dye from water and wastewater is essential and necessary [37, 38]. Some characteristics of congo red is presented in Table 1. In this study, PAn/TiO₂ and PPy/TiO₂ nanocomposites were considered as two effective nano-adsorbents removing anionic dyes Congo red from aqueous solution. The impacts of different parameters, including adsorbent dose, pH of the solution, contact time, initial dye concentration, and temperature on CR adsorption were scrutinized. Moreover, Kinetic, Isotherm, and Thermodynamic studies of CR adsorption were also carried out for the purpose of gaining a better understanding of adsorption characteristics.

2. EXPERIMENTAL

2. 1. Synthesis of Nano-adsorbents The procedure used for the synthesis of PPy/TiO₂ nanocomposite has been previously reported [39]. In order to prepare PAn/TiO₂, 2.5 g of ammonium peroxydisulfate, as an oxidizing agent, was added to 100 ml of 1M sulfuric acid containing Sodium dodecylbenzenesulfonates (0.4 g) as a surfactant and 0.1 g of titanium dioxide nanoparticles. The solution was stirred by a magnetic stirrer for 30 minutes. Afterwards, 2 ml of aniline monomer, which was distilled once prior to use, was added drop-wise to the solution. The process of nanocomposite formation was characterized by the change of color to a dark solution. It was filtered after 5 hr. The final product to be used as an adsorbent features beads connected to each other and changes into a fine powder.

2. 2. CR Adsorption Experiment Different parameters of the study, including adsorbent dose, pH of the solution, contact time, initial dye concentration, and temperature were changed, and their impacts on the efficiency of different nano-adsorbents in removing CR from the solution was investigated. The impact of different parameters on CR removal efficiency was investigated by keeping four parameters constant and changing one.

TABLE 1. Some characteristics of Congo red [40]

Chemical formula	C ₃₂ H ₂₂ N ₆ O ₆ S ₂ ·2Na
Chemical structure	
Molecular weight	696.66 g/mol
λ_{max} (nm)	496

Then, kinetic, isotherm, and thermodynamic studies of CR adsorption were also carried out. In all the experiments, solution volume was 50 ml and stirring speed was 500 rpm. Sulfuric acid and sodium hydroxide were used to change the solution pH and create acid-alkalin environment, respectively. A certain amount of adsorbent powder was added to the initial solution with certain CR concentration. The mixture was next stirred using a magnetic stirrer for a specified time so that the adsorbent was fully exposed to the adsorbate. Afterwards, the solution was filtered, and the concentration of the remaining dye in solution was determined by a UV-Vis spectrophotometer at 496 nm maximum wavelength. CR removal efficiency was determined by the following equation:

$$(\%) = (C_i - C_f) / C_i \times 100 \quad (1)$$

where, C_i (mg/l) and C_f (mg/l) were the initial and final CR concentrations, respectively. q_t (mg/g) and q_e (mg/g) are CR adsorption capacity at time (t) and the amount of adsorption at equilibrium, respectively, which were calculated based on the formula:

$$q_t = (C_i - C_t) \times \frac{V}{m}, \quad q_e = (C_i - C_e) \times \frac{V}{m} \quad (2)$$

where, C_t is the concentration of the CR at time (t); V (ml) is the volume of the solution; m (gr) is the adsorbent mass, and C_e (mg/l) is the equilibrium concentration of the CR.

3. RESULTS AND DISCUSSION

3.1. Characterization of Nano-adsorbents

The morphology of the synthesized nano-adsorbents were investigated using Scanning Electron Microscopy (SEM). Figures 1a and 1b depict the SEM images of PAn/TiO₂ and PPy/TiO₂ nano-adsorbents. As it is shown in the figures, the synthesized adsorbent particles feature nano-scaled size, uniform distribution, and spherical shape. The average size of PAn/TiO₂ nanocomposite was 58 nm and that of PPy/TiO₂ nanocomposite was found to be 102 nm. The produced adsorbent particles were very small due to the presence of stabilizers in the synthesis environment. The stabilizer can either form a chemical bond with polymer or be physically adsorbed, consequently preventing the excessive growth of the polymer chain and accumulated mass of particles during polymerization. Therefore, smaller adsorbent particles with more uniform distribution and spherical shape will be produced, which have higher specific surface area, and consequently higher adsorption capacity. Measurement software was used to measure the average particle size of PAn/TiO₂ and PPy/TiO₂ nano-adsorbents. For this purpose, about 35-40 particles of each nano-adsorbent was chosen and average particle size was calculated by software. Fourier

Transform Infrared Spectroscopy (FTIR) was applied to ensure the formation of the nano-adsorbents and examine their chemical structure. Figures 2, 3a and 3b, respectively, present the infrared spectrum of TiO₂ nanoparticles and the synthesized PAn/TiO₂ and PPy/TiO₂ nano-adsorbents within the range of 450-4000 Cm^{-1} . The large peak at the wavelength 669 Cm^{-1} was ascribed to Ti-O bond (Figure 2). As Figure 3a shows, the FTIR spectrum of PAn/TiO₂ features peaks at wavelength 1561, 1478, 1302, 1135, 809 Cm^{-1} ascribed to (C=C stretching vibration of the quinoid ring), (C=C stretching vibration of the benzenoid ring), (C-N stretching vibration), (C-H in-plane deformation), and (C-H out-of-plane deformation), and the FTIR spectrum of PPy/TiO₂ (Figure 3b) involves peaks at wavelength 1534, 1289, 1160, 1030, 887 Cm^{-1} attributed to pyrrole rings, (C-N stretching vibration), (C-H in-plane deformation), (N-H in-plane deformation), (C-H out-of-plane deformation). Furthermore, peaks at wavelength 635 Cm^{-1} and 674 Cm^{-1} were ascribed to Ti-O bond, which indicates the presence of TiO₂ nanoparticles in the above-mentioned nanocomposites.

3.2. The Effect of Adsorbent Dose on CR Adsorption

In order to investigate the effects of adsorbent dose, different amounts of nano-adsorbent (0.02-0.2 gr) were added to 50 ml of 30 mg/L dye solution. The effect of adsorbent dose on CR adsorption percentage was shown in Figure 4.

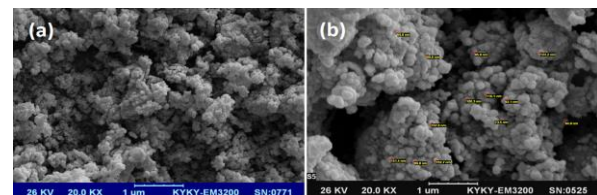


Figure 1. SEM of (a) PAn/TiO₂ and (b) PPy/TiO₂

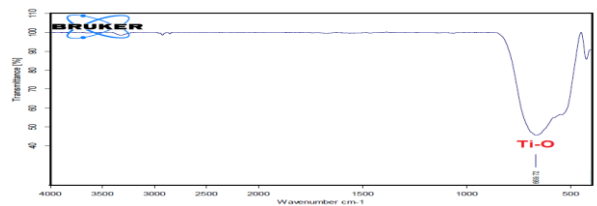


Figure 2. FTIR of TiO₂ nanoparticles

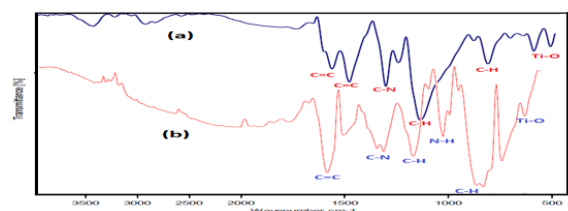


Figure 3. FTIR of (a) PAn/TiO₂ and (b) PPy/TiO₂

As the figure shows, an increase in adsorbent dose leads to a rise in the adsorption efficiency of both nano-adsorbents. CR adsorption percentage per 0.1 g adsorbent dose was measured 99.02% and 89.83% using PAn/TiO₂ and PPy/TiO₂ nano-adsorbents, respectively. When 0.2 g of PPy/TiO₂ nano-adsorbent was used, adsorption percentage reached 98.12%. The optimum adsorbent dose of PAn/TiO₂ and PPy/TiO₂ nanocomposites were considered to be 0.1 g and 0.2 g, respectively.

3. 3. The Effect of pH on CR Adsorption

The present study investigated the effect of solution pH on CR adsorption percentage of the two nano-adsorbents. In so doing, the range of pH was considered to be 2-9.5. The results obtained from pH change and its effect on adsorption efficiency were illustrated in Figure 5. As it is shown in the figure, the adsorption percentage of both nano-adsorbents decreased in the solutions with higher pH. An increase in the solution pH (alkaline condition) leads to an increase in the negative charge density of the adsorbents surface area. The electrostatic repulsion between the negatively charged pigment and negatively charged surface of the adsorbents reduces CR adsorption. However, as the figure shows, decreasing the solution pH (from 9.5 to 2) and providing acidic condition increases the adsorption efficiency of both adsorbents; the reason might lie in the fact that at low pH, active sites in the structure of nano-adsorbents can be protonated. As a result, the positive charge density of adsorbents surface area increases, and consequently, CR adsorption efficiency increases due to electrostatic attraction. As the figure shows, the adsorption efficiency of both adsorbents is high at pH less than 6. As in the range pH=2-6 no significant change occurs, further experiments were carried out at pH=6 (natural solution pH) as an optimum pH.

3. 4. The Effects of Contact Time on CR Adsorption

Figure 6 illustrates the effect of contact time on CR adsorption efficiency of the two nano-adsorbents. The contact time was changed from 1 to 60 minutes. As the figure shows, an extended contact time leads to an increase in the adsorption efficiency of both nano-adsorbents. Regarding PAn/TiO₂ nano-adsorbent, increasing the contact time from 1 min to 20 min causes the removal efficiency to increase from 94.14% to 99.02% and remain constant afterwards.

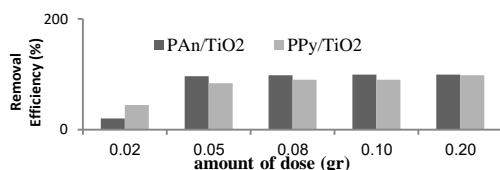


Figure 4. Effect of adsorbent dose on removal efficiency

As a result, the optimum adsorption time of this nano-adsorbent was determined to be 20 minutes. Moreover, 98.29% of CR was adsorbed within 8 minutes, which demonstrate that this adsorbent is capable of adsorbing CR in a short period of time. Figure 7 depicts PAn/TiO₂ removing CR within different contact time, i.e. 1 min, 8 min, and 20 min. As for PPy/TiO₂, an increase in contact time from 1 min to 60 min increases removal efficiency of the nano-adsorbent from 85.6% to 98.12%. Thus, the optimum adsorption time of this nano-adsorbent was considered to be 60 min.

3. 5. Adsorption Kinetics

The study of adsorption kinetics describes the adsorbate uptake rate which controls the residence time of adsorbate uptake at the solid-solution interface. The adsorption kinetics was investigated using the pseudo-first-order, pseudo-second-order, and Weber–Morris equations. The pseudo-first-order equation introduced by Lagergren in 1898 [41], describes the adsorption of liquid-solid systems based on solid capacity. This model is based on the assumption that the rate of the change of adsorbate uptake with passing of time is straightly proportional to the difference in saturation concentration and the rate of solid uptake with time. pseudo-first-order equation is expressed as follows:

$$\log(q_e - q_t) = \log q_e - \left(\frac{K_1}{2.303}\right) t \quad (3)$$

where, q_e (mg/g) and q_t (mg/g) are the amount of CR adsorbed at equilibrium and at time (t); and K_1 is the pseudo-first-order rate constant; Figures 8a and 8b depict the plots of the pseudo-first-order model for CR adsorption through PAn/TiO₂ and PPy/TiO₂.

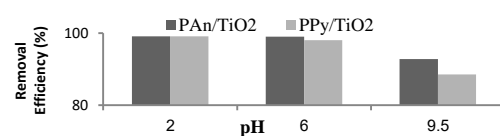


Figure 5. Effect of pH on Removal Efficiency

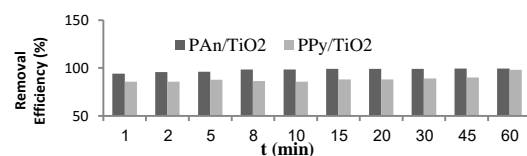


Figure 6. Effect of contact time on Removal Efficiency

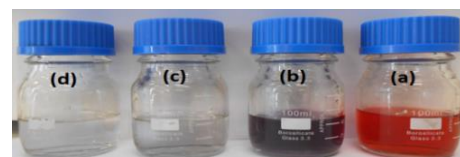


Figure 7. CR solution (a) before adsorption, (b) after adsorption with contact time: 1min, (c) 8min and (d) 20 min. (adsorbent: PAn/TiO₂)

The pseudo-first-order rate constants of CR adsorption were presented in Table 2.

The kinetic data of CR adsorption were also investigated using pseudo-second-order model. This kinetic model assumes that the process of adsorption of adsorbate (CR) is chemisorption. Pseudo-second-order model is expressed as follows [42]:

$$\frac{t}{qt} = \frac{1}{K_2 q_e^2} + \frac{1}{q_e} t \tag{4}$$

where, K_2 is the pseudo-second-order rate constant. The plots of pseudo-second-order model for CR adsorption through PAn/TiO₂ and PPy/TiO₂ nano-adsorbents were presented in Figures 9a and 9b.

In order to determine whether intraparticle diffusion is a rate-controlling step in CR adsorption, intraparticle diffusion (Weber-Morris) model was applied for the analysis of the kinetic data. The intraparticle diffusion model introduced by Weber and Morris is expressed as follows [43]:

$$q_t = K_{id}(t)^{0.5} + C \tag{5}$$

where, K_{id} is the intraparticle diffusion rate constant; and C is a constant that gives an idea about the thickness of the boundary layer.

TABLE 2. Kinetic constants for Congo Red adsorption

Pseudo-second order	Pseudo-first order	Weber-Morris
PAn/TiO₂:	PAn/TiO₂:	PAn/TiO ₂ :
K_2 : 0.6906154	K_1 : 0.2606996	K_{id} = 0.1014
q_e : 14.925373	q_e : 1.0413578	C=14.276
q_e^* : 14.85347985	R^2 : 0.9715	R^2 : 0.6811
R^2 : 1		
PPy/TiO₂:	PPy/TiO₂:	PPy/TiO ₂ :
K_2 : 0.131356	K_1 : 0.0099029	K_{id} =0.1067
q_e : 7.23589	q_e : 0.928111171	C=6.2172
q_e^* : 7.358974359	R^2 : 0.8654	R^2 : 0.7223
R^2 : 0.9953		
q_e^* : Experimental		

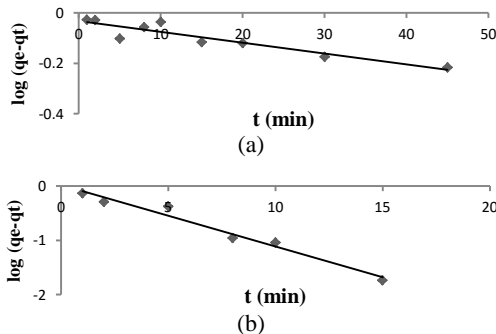


Figure 8. Pseudo-first-order plot of CR adsorption on (a) PAn/TiO₂ and (b) PPy/TiO₂

If the plot (q_t vs. $t^{0.5}$) is linear, the process of CR adsorption is controlled by diffusion resistance. The plots (q_t vs. $t^{0.5}$) for CR adsorption onto the two nano-adsorbents were presented in Figures 10a and 10b. The slope and intercept of the plot can be used to derive values for the constants K_{id} and C, respectively. The values were shown in Table 2. The correlation (R^2) of the three kinetic models, i.e. pseudo-first-order, pseudo-second-order, and Weber-Morris equations for PAn/TiO₂ nanocomposite was measured as 0.9715, 1, and 0.6811, respectively. As for PPy/TiO₂ nanocomposite, the values were calculated as 0.8654, 0.9953, and 0.7223, respectively (Table 2). The experimental data were well described by the pseudo-second-order kinetic model, which indicates that the process of CR adsorption onto both nano-adsorbents is chemisorption-controlled. Furthermore, CR adsorption capacity of both nano-adsorbents obtained through pseudo-second-order kinetic model was very close to its experimental value.

3. 6. The Effect of the Initial Concentration on CR Adsorption Capacity

In order to scrutinize the effect of the initial concentration on adsorption capacity, CR solutions with the initial concentration of 30-100 mg/L were provided. The plot of the adsorption capacity based on the initial concentration of dye solution was presented in Figure 11. The adsorption capacity of both nano-adsorbents increased with increasing the initial concentration.

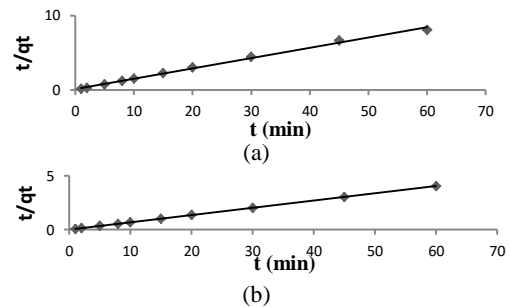


Figure 9. Pseudo-second-order plot of CR adsorption on (a) PAn/TiO₂ and (b) PPy/TiO₂

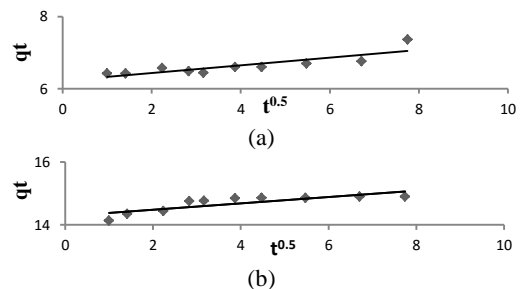


Figure 10. Weber-Morris plot of CR adsorption on (a) PAn/TiO₂ and (b) PPy/TiO₂

3. 7. Isotherm Models Isotherm equations describe the relationship between dye concentration in solution and the amount of dye adsorbed on the solid phase at equilibrium. The present study assessed CR adsorption data using four isotherms, namely Langmuir, Freundlich, Temkin, and D-R. In Langmuir isotherm, adsorption energy is independent of surface coverage; there is a uniform surface with equivalent adsorption sites; and each adsorption site can simply adsorb one species. Moreover, the adsorption is limited to a monolayer. Langmuir isotherm is expressed as follows [44]:

$$q_e = \frac{q_m K_L C_e}{1 + K_L C_e} \tag{6}$$

q_e is the amount of CR adsorbed per unit weight of nano-adsorbent (mg/g); C_e is the equilibrium solution concentration (mg/l); q_m is the maximum adsorption capacity; and K_L is equilibrium constant. Langmuir isotherm can be linearized as follow:

$$\frac{C_e}{q_e} = \frac{1}{q_m K_L} + \frac{1}{q_m} C_e \tag{7}$$

Linear Langmuir plot can be used to derive the values of maximum adsorption capacity and equilibrium constant. This plot for PAn/TiO₂ and PPy/TiO₂ nano-adsorbents was illustrated in Figures 12a and 12b, respectively. The value of the maximum CR adsorption capacity and equilibrium constant, obtained from the Linear Langmuir equation were presented in Table 3. As can be seen, CR adsorption data on PPy/TiO₂ nanocomposite, does not fit to the Langmuir isotherm, because the slope of line is negative [45]. R_L is a dimensionless constant and expresses the essential features of the Langmuir isotherm [46]:

$$R_L = \frac{1}{1 + K_L C_i} \tag{8}$$

C_i is the initial concentration; and K_L is Langmuir constant. As the R_L values calculated in the range 0-1, adsorption process onto adsorbent is favorable.

Freundlich isotherm is an empirical equation. It is used for heterogeneous surface energies and multilayer adsorption. This equation does not predict the maximum adsorption and is expressed as follows [47]:

$$q_e = K_F (C_e)^{1/n} \tag{9}$$

where, K_F is Freundlich constant; and $1/n$ is adsorption intensity which obtained from the intercept and the slope of the linearized plots of $\log(q_e)$ versus $\log(C_e)$.

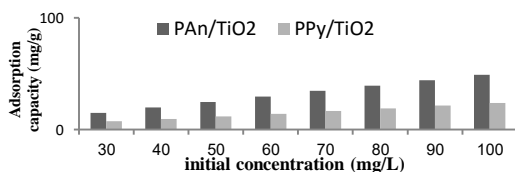


Figure 11. Effect of Initial Concentration on adsorption capacity

TABLE 3. Isotherm constants for Congo Red adsorption

Langmuir	Freundlich	Tempkin	D-R
PAn/TiO₂: K _L : 0.6813 q _m (mg/g)= 80.645 R _L :0.014465- 0.046644 R ² : 0.945	PAn/TiO₂: K _F : 31.3834 n:1.62285 R ² : 0.9759	PAn/TiO₂: B:17.77 K _T :6.5566 R ² : 0.9631	PAn/TiO ₂ : β=4×10 ⁻⁹ X _m =94.94 E=11.18 R ² : 0.816
PPy/TiO₂: K _L : -0.08988 q _m (mg/g)= -29.154 R _L :(-0.58948)- (0.12518), R ² : 0.6444	PPy/TiO₂: K _F : 2.10329 n: 0.67024 R ² : 0.9301	PPy/TiO₂: B: 22.392 K _T : 0.54182 R ² : 0.8643	PPy/TiO ₂ : β=6×10 ⁻⁹ X _m =50.14 E= 9.128 R ² : 0.6644

The plots of Freundlich model were presented in Figures 13a and 13b. Temkin Isotherm contains a factor that expresses adsorbent–adsorbate interactions. Temkin equation is described as follows [48]:

$$q_e = \frac{RT}{b_T} \ln(K_T C_e) \tag{11}$$

The above equation can be linearized as:

$$q_e = B \ln(K_T) + B \ln(C_e) \tag{12}$$

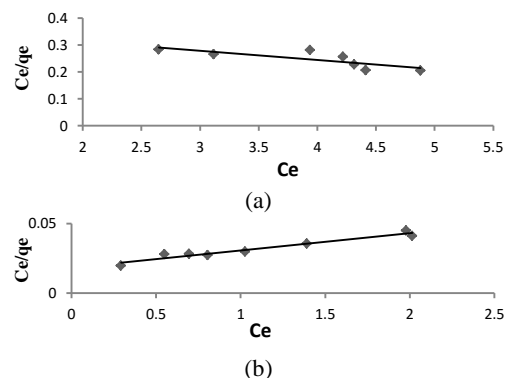


Figure 12. Langmuir adsorption isotherm of Congo Red on (a) PAn/TiO₂ and (b) PPy/TiO₂

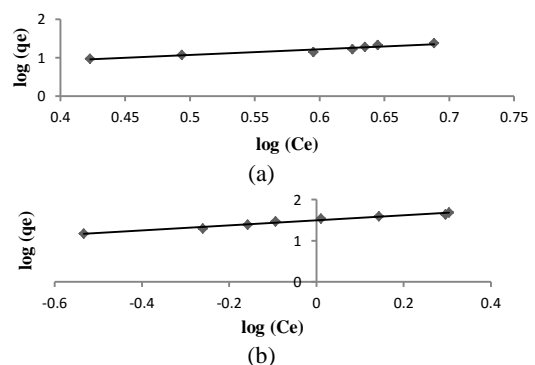


Figure 13. Freundlich adsorption isotherm of Congo Red on (a) PAn/TiO₂ and (b) PPy/TiO₂

In which $B = \frac{RT}{b}$ is defined. Here, K_T is Temkin isotherm equilibrium binding constant (L/g); b_T is Temkin isotherm constant; R is the universal gas constant (8.314 J/mol.K); T is temperature in Kelvin (293.15 K); and B is constant related to the adsorption heat (J/mol). B and K_T values can be calculated via q_e versus $\ln(C_e)$ plot (Figures 14a and 14b). B and K_T values for the two nano-adsorbents were shown in Table 3.

D-R isotherm [49] is used to express the type of CR adsorption (physical or chemical). The linear form of model is presented in the following equation:

$$\ln(q_e) = \ln(X_m) - \beta \varepsilon^2 \tag{13}$$

where, ε is the Polanyi potential; X_m is the maximum of adsorption capacity and β is the constant related to the adsorption energy; ε is presented as:

$$\varepsilon = RT \ln\left(1 + \frac{1}{C_e}\right) \tag{14}$$

Figures 15a and 15b illustrate $\ln(q_e)$ vs. ε^2 plots for the two nano-adsorbents. Isotherm constant (β), calculated by the slope of the plots. The average adsorption energy, E , (kJ/mol) obtained by β is calculated by the following equation:

$$E = (2\beta)^{-0.5} \tag{15}$$

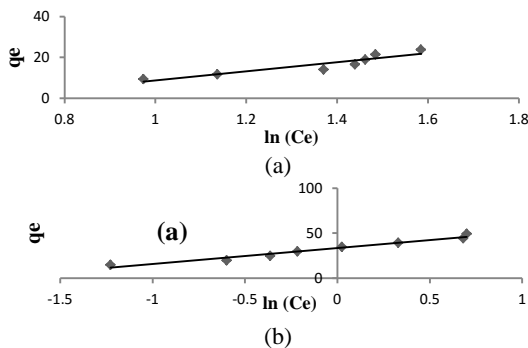


Figure 14. Temkin adsorption isotherm of Congo Red on (a) PAN/TiO₂ and (b) PPy/TiO₂

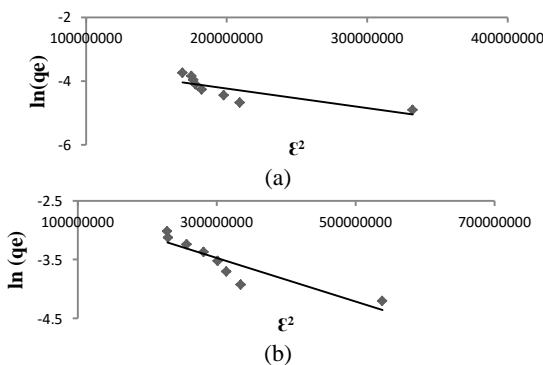


Figure 15. D-R adsorption isotherm of Congo Red on (a) PAN/TiO₂ and (b) PPy/TiO₂

If the magnitude of E is between 8 and 16 kJ/mol, the adsorption process is regarded as chemisorption whereas if it is less than 8 kJ/mol, the adsorption process is of physical nature.

The results of the study confirmed that the process of CR adsorption onto both nano-adsorbents is chemisorption. The results obtained using isotherm studies are depicted in Table 2. It can be claimed that Freundlich adsorption isotherm shows a better fit to CR adsorption data than the other isotherms.

3. 8. Thermodynamic Studies of Adsorption Process

In order to evaluate the effect of temperature on the adsorption of Congo red, adsorption experiments were carried out at 20-60°C. The results of temperature change and its effect on CR adsorption efficiency were illustrated in Table 4. As the table shows, an increase in temperature decreases the adsorption efficiency of both nano-adsorbents. This result indicates that CR adsorption onto both nano-adsorbents is exothermic in nature. The results of the experiments on the effect of temperature on CR adsorption as well as the Equations (16) to (18) were used to evaluate thermodynamic parameters, i.e. Gibbs free energy change (ΔG), the enthalpy change (ΔH), and the entropy change (ΔS) [50]:

$$K_C = \frac{F_e}{1-F_e} \tag{16}$$

$$\ln(k_C) = \frac{-\Delta H}{RT} + \frac{\Delta S}{R} \tag{17}$$

$$\Delta G = -RT \ln(k_C) \tag{18}$$

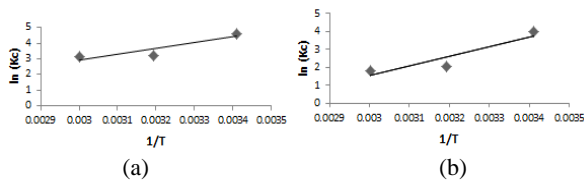
where, F_e is the fraction of adsorbed dye at equilibrium; R is the universal gas constant (8.314J/mol.K); T is temperature in Kelvin; and k_C is thermodynamic equilibrium constant. The enthalpy change (ΔH) and entropy change (ΔS) values of CR adsorption for both nano-adsorbents were obtained from the slope and intercept of $\ln(k_C)$ vs. $\frac{1}{T}$ plot, respectively (Figures 16a and 16b). The values were presented in Table 5. As the table shows, the negative value of the enthalpy change (ΔH) is indicative of the exothermic nature of the CR adsorption. Furthermore, the negative value of Gibbs free energy change (ΔG) implies the spontaneity of CR adsorption process.

3. 9. Comparing PAN/TiO₂ with the Other Adsorbents

The maximum CR adsorption capacity of PAN/TiO₂ nano-adsorbent obtained from Langmuir isotherm model was compared with that of the adsorbents applied in the other studies. The results were presented in Table 6. As the table shows, the adsorption capacity of the nano-adsorbent used in the present study is comparable to that of the adsorbents applied in the other studies.

TABLE 4. Effect of temperature on adsorption of CR

adsorbent	Temperature (°C)	Removal efficiency (%)
PAn/TiO ₂	20	99.023
	40	96.215
	60	95.848
PPy/TiO ₂	20	98.119
	40	88.608
	60	86.080

**Figure 16.** $\ln(k_C)$ vs. $\frac{1}{T}$ for CR adsorption process on (a) PAn/TiO₂ and (b) PPy/TiO₂**TABLE 5.** Thermodynamic parameters of CR adsorption

adsorbent	Temperature (°C)	ΔG ($\frac{KJ}{mol}$)	ΔH ($\frac{KJ}{mol}$)	ΔS ($\frac{KJ}{mol.K}$)
PAn/TiO ₂	20	-11.2572		
	40	-8.4237	-30.5472	-0.06734
	60	-8.6953		
PPy/TiO ₂	20	-9.6386		
	40	-5.3406	-43.9569	-0.11905
	60	-5.0465		

TABLE 6. Comparison of maximum adsorption capacity of various adsorbents obtained from Langmuir isotherm

Adsorbent	q_m (mg/g)	References
Fe ₃ O ₄ /graphene composite	33.66	[51]
Fe-Zn nanoparticles	28.56	[52]
Iron-grafted clinoptilolite	36.70	[53]
MnFe ₂ O ₄ nanoparticles	41.99	[54]
MnFe ₂ O ₄ /PW composite	86.96	[38]
Hierarchically structured γ -ALOOH	99	[55]
Luffa cylindrica cellulosic fibre	17.39	[56]
Apricot stone activated carbon	32.852	[57]
Cetyltrimethyl ammonium bromide modified pumice	27.32	[40]
ZrO ₂ hollow spheres	59.5	[58]
PAn/TiO ₂ nanocomposite	80.645	This study

4. CONCLUSION

In this study, PAn/TiO₂ and PPy/TiO₂ nanocomposites were synthesized through chemical polymerization and used as adsorbents of Congo red from aqueous solution. The study yielded the result that CR adsorption was influenced by environment pH, that is, a decrease in pH increases the adsorption efficiency of both nano-adsorbents. The adsorbent dose and optimum contact time of PAn/TiO₂ and PPy/TiO₂ were [0.1 gr, 20 min] and [0.2 gr, 60 min], respectively. When the initial concentration of the solution changed from 30 mg/L to 100 mg/L, the adsorption capacity of PAn/TiO₂ increased from 14.85 to 48.99 mg/g, and that of PPy/TiO₂ rised 7.35 to 23.78 mg/g. The kinetic data suggested that the adsorption process was controlled by pseudo-second-order equation, which indicates that the adsorption is chemisorption in nature. The constants of Langmuir, Freundlich, Temkin, and D-R isotherms were calculated for CR adsorption onto the two nano-adsorbents. The results revealed that the experimental data were best represented by Freundlich isotherm model compared to the other models. The results obtained from D-R isotherm confirmed that the process of CR adsorption onto both nano-adsorbents is of chemical nature. Also, the results of thermodynamic studies demonstrated that CR adsorption onto both nano-adsorbents was exothermic and spontaneous.

5. REFERENCES

- Arslan, I., Balcioglu, I.A. and Bahnemann, D.W., "Advanced chemical oxidation of reactive dyes in simulated dyehouse effluents by ferrioxalate-fenton/UV-A and TiO₂/uv-a processes", *Dyes and pigments*, Vol. 47, No. 3, (2000), 207-218.
- Daneshvar, N., Salari, D. and Khataee, A., "Photocatalytic degradation of AZO dye acid red 14 in water: Investigation of the effect of operational parameters", *Journal of Photochemistry and Photobiology A: Chemistry*, Vol. 157, No. 1, (2003), 111-116.
- de Lima, R.O.A., Bazo, A.P., Salvadori, D.M.F., Rech, C.M., de Palma Oliveira, D. and de Aragao Umbuzeiro, G., "Mutagenic and carcinogenic potential of a textile AZO dye processing plant effluent that impacts a drinking water source", *Mutation Research/Genetic Toxicology and Environmental Mutagenesis*, Vol. 626, No. 1, (2007), 53-60.
- Pearce, C., Lloyd, J. and Guthrie, J., "The removal of colour from textile wastewater using whole bacterial cells: A review", *Dyes and pigments*, Vol. 58, No. 3, (2003), 179-196.
- Ramallo, P.A., "Degradation of dyes with microorganisms: Studies with ascomycete yeasts", Vol., No., (2005).
- Tian, J., Xu, J., Zhu, F., Lu, T., Su, C. and Ouyang, G., "Application of nanomaterials in sample preparation", *Journal of Chromatography A*, Vol. 1300, (2013), 2-16.
- El-Nahhal, I.M., Zourab, S.M., Kodeh, F.S., Elmanama, A.A., Selmane, M., Genois, I. and Babonneau, F., "Nano-structured zinc oxide-cotton fibers: Synthesis, characterization and applications", *Journal of Materials Science: Materials in Electronics*, Vol. 24, No. 10, (2013), 3970-3975.

8. Yan, X., Shi, B., Lu, J., Feng, C., Wang, D. and Tang, H., "Adsorption and desorption of atrazine on carbon nanotubes", *Journal of Colloid and Interface Science*, Vol. 321, No. 1, (2008), 30-38.
9. Yusan, S., Korzhynbayeva, K., Aytas, S., Tazhibayeva, S. and Musabekov, K., "Preparation and investigation of structural properties of magnetic diatomite nanocomposites formed with different iron content", *Journal of Alloys and Compounds*, Vol. 608, (2014), 8-13.
10. Zhang, W. and Wang, C., "Nanoscale metal particles for dechlorination of pce and pcbs", *Environmental Science and Technology*, Vol. 31, No. 7, (1997), 2154-2156.
11. Xu, Y. and Zhang, W.-x., "Subcolloidal Fe/Ag particles for reductive dehalogenation of chlorinated benzenes", *Industrial & Engineering Chemistry Research*, Vol. 39, No. 7, (2000), 2238-2244.
12. Asfaram, A., Ghaedi, M., Hajati, S., Goudarzi, A. and Dil, E.A., "Screening and optimization of highly effective ultrasound-assisted simultaneous adsorption of cationic dyes onto mn-doped Fe₃O₄-nanoparticle-loaded activated carbon", *Ultrasonics Sonochemistry*, Vol. 34, No., (2017), 1-12.
13. Fayazi, M., Ghanei-Motlagh, M. and Taher, M.A., "The adsorption of basic dye (alizarin red s) from aqueous solution onto activated carbon/ γ - Fe₃O₄ nano-composite: Kinetic and equilibrium studies", *Materials Science in Semiconductor Processing*, Vol. 40, No., (2015), 35-43.
14. Salem, A.-N.M., Ahmed, M. and El-Shahat, M., "Selective adsorption of amaranth dye on Fe₃O₄/MgO nanoparticles", *Journal of Molecular Liquids*, Vol. 219, (2016), 780-788.
15. Ali, I., AL-Othman, Z.A. and Alwarthan, A., "Green synthesis of functionalized iron nano particles and molecular liquid phase adsorption of ametryn from water", *Journal of Molecular Liquids*, Vol. 221, No., (2016), 1168-1174.
16. Hashemian, S., Dehghanpor, A. and Moghahed, M., "Cu_{0.5}Mn_{0.5}Fe₂O₄ nano spinels as potential sorbent for adsorption of brilliant green", *Journal of Industrial and Engineering Chemistry*, Vol. 24, No., (2015), 308-314.
17. Sun, H., She, P., Xu, K., Shang, Y., Yin, S. and Liu, Z., "A self-standing nanocomposite foam of polyaniline@ reduced graphene oxide for flexible super-capacitors", *Synthetic Metals*, Vol. 209, No., (2015), 68-73.
18. Pandey, S. and Ramontja, J., "Rapid, facile microwave-assisted synthesis of xanthan gum grafted polyaniline for chemical sensor", *International journal of biological macromolecules*, Vol. 89, No., (2016), 89-98.
19. Kim, B., Koncar, V. and Dufour, C., "Polyaniline-coated pet conductive yarns: Study of electrical, mechanical, and electro-mechanical properties", *Journal of Applied Polymer Science*, Vol. 101, No. 3, (2006), 1252-1256.
20. Bhaumik, M., McCrindle, R.I., Maity, A., Agarwal, S. and Gupta, V.K., "Polyaniline nanofibers as highly effective reusable adsorbent for removal of reactive black 5 from aqueous solutions", *Journal of Colloid and Interface Science*, Vol. 466, No., (2016), 442-451.
21. Focke, W.W., "Conduction mechanisms in polyaniline", Massachusetts Institute of Technology, (1987),
22. Raghavan, M. and Trivedi, D., "Use of polyaniline in lead-acid battery", *Synthetic Metals*, Vol. 119, No. 1, (2001), 285-286.
23. Waltman, R.J. and Bargon, J., "Reactivity/structure correlations for the electropolymerization of pyrrole: An INDO/CNDO study of the reactive sites of oligomeric radical cations", *Tetrahedron*, Vol. 40, No. 20, (1984), 3963-3970.
24. Ruckenstein, E. and Chen, J.-H., "Polypyrrole conductive composites prepared by coprecipitation", *Polymer*, Vol. 32, No. 7, (1991), 1230-1235.
25. Weidlich, C., Mangold, K.-M. and Jüttner, K., "Conducting polymers as ion-exchangers for water purification", *Electrochimica Acta*, Vol. 47, No. 5, (2001), 741-745.
26. Shanehsaz, M., Seidi, S., Ghorbani, Y., Shoja, S.M.R. and Rouhani, S., "Polypyrrole-coated magnetic nanoparticles as an efficient adsorbent for RB19 synthetic textile dye: Removal and kinetic study", *Spectrochimica Acta Part A: Molecular and Biomolecular Spectroscopy*, Vol. 149, No., (2015), 481-486.
27. Salem, M.A., Elsharkawy, R.G. and Hablas, M.F., "Adsorption of brilliant green dye by polyaniline/silver nanocomposite: Kinetic, equilibrium, and thermodynamic studies", *European Polymer Journal*, Vol. 75, (2016), 577-590.
28. Khalili, R. and Eisazadeh, H., "Preparation and characterization of polyaniline/ Sb₂O₃ nanocomposite and its application for removal of pb (II) from aqueous media", *International Journal of Engineering-Transactions B: Applications*, Vol. 27, No. 2, (2013), 239-246.
29. Leong, S., Razmjou, A., Wang, K., Hapgood, K., Zhang, X. and Wang, H., "TiO₂ based photocatalytic membranes: A review", *Journal of Membrane Science*, Vol. 472, (2014), 167-184.
30. Alev, O., Sennik, E., Kilinc, N. and Ozturk, Z.Z., "Gas sensor application of hydrothermally growth tio 2 nanorods", *Procedia Engineering*, Vol. 120, (2015), 1162-1165.
31. Boroumandnia, A., Kasaeian, A., Nikfarjam, A. and Mohammadpour, R., "Effect of TiO₂ nanofiber density on organic-inorganic based hybrid solar cells", *International Journal of Engineering*, Vol. 1025, No. 2495, (2014), 1133-1138.
32. Kashale, A.A., Gattu, K.P., Ghule, K., Ingole, V.H., Dhanayat, S., Sharma, R., Chang, J.-Y. and Ghule, A.V., "Biomediated green synthesis of TiO₂ nanoparticles for lithium ion battery application", *Composites Part B: Engineering*, (2016).
33. Akhlaghian, F. and Sohrabi, S., "Fe/TiO₂ catalyst for photodegradation of phenol in water", *IJE Transactions A: Basics*, Vol. 28, (2015), 499-506.
34. Skoric, M.L., Terzic, I., Milosavljevic, N., Radetic, M., Saponjic, Z., Radoicic, M. and Krusic, M.K., "Chitosan-based microparticles for immobilization of TiO₂ nanoparticles and their application for photodegradation of textile dyes", *European Polymer Journal*, Vol. 82, No., (2016), 57-70.
35. Roux, S., de AA Soler-Illia, G., Demoustier-Champagne, S., Audebert, P. and Sanchez, C., "Titania/polypyrrole hybrid nanocomposites built from in-situ generated organically functionalized nanoanatase building blocks", *Advanced Materials*, Vol. 15, No. 3, (2003), 217-221.
36. Deivanayaki, S., Ponnuswamy, V., Ashokan, S., Jayamurugan, P. and Mariappan, R., "Synthesis and characterization of TiO₂-doped polyaniline nanocomposites by chemical oxidation method", *Materials Science in Semiconductor Processing*, Vol. 16, No. 2, (2013), 554-559.
37. Mall, I.D., Srivastava, V.C., Agarwal, N.K. and Mishra, I.M., "Removal of congo red from aqueous solution by bagasse fly ash and activated carbon: Kinetic study and equilibrium isotherm analyses", *Chemosphere*, Vol. 61, No. 4, (2005), 492-501.
38. Saygili, G.A., "Synthesis, characterization and adsorption properties of a novel biomagnetic composite for the removal of congo red from aqueous medium", *Journal of Molecular Liquids*, Vol. 211, (2015), 515-526.
39. Tanzifi, M., Kolaei, Z.T. and Roushani, M., "Characterization of polypyrrole-hydroxyethylcellulose/tio2 nanocomposite: Thermal properties and afm analysis", *International Journal of Engineering-Transactions B: Applications*, Vol. 28, No. 5, (2014), 654.
40. Shayesteh, H., Rahbar-Kelishami, A. and Norouzbeigi, R., "Evaluation of natural and cationic surfactant modified pumice

- for congo red removal in batch mode: Kinetic, equilibrium, and thermodynamic studies", *Journal of Molecular Liquids*, Vol. 221, (2016), 1-11.
41. Lagergren, S., "About the theory of so-called adsorption of soluble substances", (1898).
 42. Ho, Y.-S. and McKay, G., "Pseudo-second order model for sorption processes", *Process biochemistry*, Vol. 34, No. 5, (1999), 451-465.
 43. Weber, W.J. and Morris, J.C., "Kinetics of adsorption on carbon from solution", *Journal of the Sanitary Engineering Division*, Vol. 89, No. 2, (1963), 31-60.
 44. Langmuir, I., "The constitution and fundamental properties of solids and liquids. Part i. Solids", *Journal of the American Chemical Society*, Vol. 38, No. 11, (1916), 2221-2295.
 45. Omraei, M., Esfandian, H., Katal, R. and Ghorbani, M., "Study of the removal of Zn (II) from aqueous solution using polypyrrole nanocomposite", *Desalination*, Vol. 271, No. 1, (2011), 248-256.
 46. Weber, T.W. and Chakravorti, R.K., "Pore and solid diffusion models for fixed-bed adsorbers", *AIChE Journal*, Vol. 20, No. 2, (1974), 228-238.
 47. Uber, F., "Die adsorption in losungen", *Zeitschrift fur Physikalische Chemie-Leipzig*, Vol. 57, (1985), 387-470.
 48. Temkin, M. and Pyzhev, V., "Kinetics of ammonia synthesis on promoted iron catalysts", *Acta physiochim. URSS*, Vol. 12, No. 3, (1940), 217-222.
 49. Dubinin, M. and Radushkevich, L., "Equation of the characteristic curve of activated charcoal", *Chem. Zentr*, Vol. 1, No. 1, (1947), 875.
 50. Javadian, H., Ghorbani, F., Tayebi, H.-a. and Asl, S.H., "Study of the adsorption of cd (ii) from aqueous solution using zeolite-based geopolymer, synthesized from coal fly ash; kinetic, isotherm and thermodynamic studies", *Arabian Journal of Chemistry*, Vol. 8, No. 6, (2015), 837-849.
 51. Yao, Y., Miao, S., Liu, S., Ma, L.P., Sun, H. and Wang, S., "Synthesis, characterization, and adsorption properties of magnetic Fe₃O₄ graphene nanocomposite", *Chemical Engineering Journal*, Vol. 184, (2012), 326-332.
 52. Gautam, R.K., Rawat, V., Banerjee, S., Sanroman, M.A., Soni, S., Singh, S.K. and Chattopadhyaya, M.C., "Synthesis of bimetallic fe-zn nanoparticles and its application towards adsorptive removal of carcinogenic dye malachite green and congo red in water", *Journal of Molecular Liquids*, Vol. 212, (2015), 227-236.
 53. Akgul, M., "Enhancement of the anionic dye adsorption capacity of clinoptilolite by Fe³⁺-grafting", *Journal of hazardous materials*, Vol. 267, (2014), 1-8.
 54. Liu, X., Zhang, Z., Shi, W., Zhang, Y., An, S. and Zhang, L., "Adsorbing properties of magnetic nanoparticles Mn-ferrites on removal of congo red from aqueous solution", *Journal of Dispersion Science and Technology*, Vol. 36, No. 4, (2015), 462-470.
 55. Meng, F., Rong, G., Zhang, X. and Huang, W., "Facile hydrothermal synthesis of hierarchically structured γ -ALOOH for fast congo red removal", *Materials Letters*, Vol. 129, (2014), 114-117.
 56. Gupta, V.K., Pathania, D., Agarwal, S. and Sharma, S., "Amputation of congo red dye from waste water using microwave induced grafted luffa cylindrica cellulosic fiber", *Carbohydrate polymers*, Vol. 111, (2014), 556-566.
 57. Abbas, M. and Trari, M., "Kinetic, equilibrium and thermodynamic study on the removal of congo red from aqueous solutions by adsorption onto apricot stone", *Process Safety and Environmental Protection*, Vol. 98, (2015), 424-436.
 58. Wang, C., Le, Y. and Cheng, B., "Fabrication of porous ZrO₂ hollow sphere and its adsorption performance to congo red in water", *Ceramics International*, Vol. 40, No. 7, (2014), 10847-10856.

Removal of Congo Red Anionic Dye from Aqueous Solution Using Polyaniline/TiO₂ and Polypyrrole/TiO₂ Nanocomposites: Isotherm, Kinetic, and Thermodynamic Studies

M. Tanzifi, K. Karimipour, M. Najafifard, S. Mirchenari

Department of Chemical Engineering, Faculty of Engineering, University of Ilam, Ilam, Iran

PAPER INFO

چکیده

Paper history:

Received 17 August 2016

Received in revised form 23 September 2016

Accepted 11 November 2016

Keywords:

Polyaniline
Polypyrrole
Titanium Dioxide
Adsorption
Kinetic Studies
Isotherm
Thermodynamic
Congo Red

در پژوهش حاضر، توانایی نانوجاذب های پلی آنیلین/دی اکسید تیتانیوم و پلی پیرول/دی اکسید تیتانیوم در جذب سطحی رنگزای آنیونی قرمز کنگو (CR) از محلول های آبی مورد بررسی قرار گرفت. تاثیر متغیرهای موثر بر فرآیند جذب سطحی CR از جمله مقدار جاذب، pH محلول، زمان تماس، غلظت اولیه رنگزا و دما بررسی شد. نتایج حاصل از پژوهش نشان داد که با کاهش pH راندمان جذب سطحی رنگزا در مورد هر دو نانوجاذب افزایش یافت. مقدار جاذب و زمان بهینه جذب برای نانوکامپوزیت های پلی آنیلین/دی اکسید تیتانیوم و پلی پیرول/دی اکسید تیتانیوم به ترتیب (۰.۱ گرم و ۲۰ دقیقه) و (۰.۲ گرم و ۶۰ دقیقه) بدست آمد. سینتیک های جذب سطحی توسط سه معادله شبه مرتبه اول، شبه مرتبه دوم و موریس وبر مورد مطالعه قرار گرفت. مطالعات سینتیکی نشان داد که فرآیند جذب سطحی CR بر روی هر دو نانوجاذب از معادله سینتیکی شبه مرتبه دوم تبعیت می کند که بیان کننده این است که فرآیند به وسیله جذب شیمیایی کنترل می شود. ایزوترم های لانگمویر، فروندلیچ، تمکین و دابینین رادشکوویچ، جهت تخمین حداکثر ظرفیت جذب، شدت و انرژی جذب برای داده های جذب سطحی بکار گرفته شدند. ایزوترم فروندلیچ بهترین همخوانی را با داده های تجربی در مقایسه با دیگر ایزوترم ها از خود نشان داد. آنالیز داده ها توسط ایزوترم دابینین رادشکوویچ نشان داد که جذب سطحی رنگ CR بر روی هر دو نانوجاذب، فرآیند شیمیایی می باشد. همچنین پارامترهای ترمودینامیکی از جمله ΔG ، ΔH و ΔS محاسبه گردیدند. نتایج نشان داد که فرآیند جذب سطحی رنگ CR بر روی هر دو نانوجاذب، خود به خودی و گرمازا می باشد.

doi: 10.5829/idosi.ije.2016.29.12c.04